Since January 2020 Elsevier has created a COVID-19 resource centre with free information in English and Mandarin on the novel coronavirus COVID-19. The COVID-19 resource centre is hosted on Elsevier Connect, the company's public news and information website.

Elsevier hereby grants permission to make all its COVID-19-related research that is available on the COVID-19 resource centre - including this research content - immediately available in PubMed Central and other publicly funded repositories, such as the WHO COVID database with rights for unrestricted research re-use and analyses in any form or by any means with acknowledgement of the original source. These permissions are granted for free by Elsevier for as long as the COVID-19 resource centre remains active.

Article

Cell

Ebola Virus Glycoprotein with Increased Infectivity Dominated the 2013–2016 Epidemic

Graphical Abstract

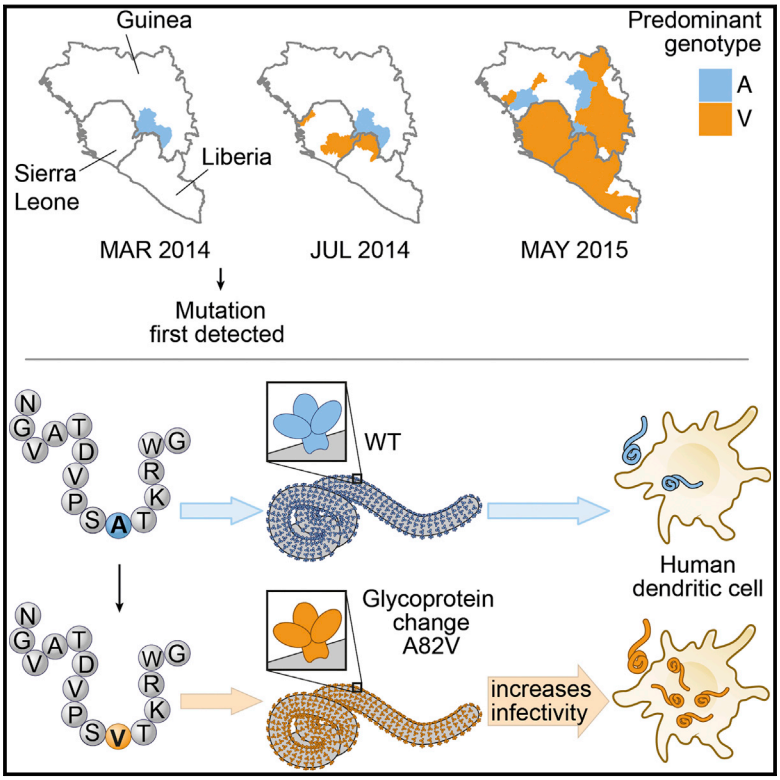

Highlights

- Ebola glycoprotein mutant GP-A82V arose early and dominated the West African epidemic
- GP-A82V infects human cells more efficiently than does the ancestral glycoprotein
- The increased infectivity of GP-A82V is specific for primate cells
- GP-A82V was weakly associated with increased mortality during the epidemic

Authors

William E. Diehl, Aaron E. Lin, Nathan D. Grubaugh, ..., Kristian G. Andersen, Pardis C. Sabeti, Jeremy Luban

Correspondence

andersen@scripps.edu (K.G.A.), pardis@broadinstitute.org (P.C.S.), jeremy.luban@umassmed.edu (J.L.)

In Brief

An Ebola glycoprotein mutant that arose early during the West African epidemic increases infectivity of human cells and may have contributed to increased mortality

Diehl et al., 2016, Cell *167*, 1088–1098
November 3, 2016 © 2016 Elsevier Inc.
http://dx.doi.org/10.1016/j.cell.2016.10.014

CellPress

Cell

Article

Ebola Virus Glycoprotein with Increased Infectivity Dominated the 2013–2016 Epidemic

William E. Diehl,[1,9] Aaron E. Lin,[2,3,9] Nathan D. Grubaugh,[4,9] Luiz Max Carvalho,[5,9] Kyusik Kim,[1] Pyae Phyo Kyawe,[6] Sean M. McCauley,[1] Elisa Donnard,[1,7] Alper Kucukural,[1,7] Patrick McDonel,[1,7] Stephen F. Schaffner,[2,3] Manuel Garber,[1,7] Andrew Rambaut,[5] Kristian G. Andersen,[2,4,8,*] Pardis C. Sabeti,[2,3,*] and Jeremy Luban[1,10,*]

[1]Program in Molecular Medicine, University of Massachusetts Medical School, 373 Plantation Street, Worcester, MA 01605, USA
[2]Broad Institute of Harvard and MIT, 75 Ames Street, Cambridge, MA 02142, USA
[3]Harvard University, 52 Oxford Street, Cambridge, MA 02138, USA
[4]Department of Immunology and Microbial Science, The Scripps Research Institute, 10550 North Torrey Pines Road, La Jolla, CA 92037, USA
[5]Institute of Evolutionary Biology, University of Edinburgh, Ashworth Laboratories, Kings Buildings, West Mains Road, Edinburgh EH9 3JT, Scotland, UK
[6]Department of Medicine, University of Massachusetts Medical School, 55 Lake Avenue North, Worcester, MA 01605, USA
[7]Program in Bioinformatics and Integrative Biology, University of Massachusetts Medical School, Worcester, MA 01655, USA
[8]Scripps Translational Science Institute, 3344 North Torrey Pines Court, La Jolla, CA 92037, USA
[9]Co-first author
[10]Lead Contact
*Correspondence: andersen@scripps.edu (K.G.A.), pardis@broadinstitute.org (P.C.S.), jeremy.luban@umassmed.edu (J.L.)
http://dx.doi.org/10.1016/j.cell.2016.10.014

SUMMARY

The magnitude of the 2013–2016 Ebola virus disease (EVD) epidemic enabled an unprecedented number of viral mutations to occur over successive human-to-human transmission events, increasing the probability that adaptation to the human host occurred during the outbreak. We investigated one nonsynonymous mutation, Ebola virus (EBOV) glycoprotein (GP) mutant A82V, for its effect on viral infectivity. This mutation, located at the NPC1-binding site on EBOV GP, occurred early in the 2013–2016 outbreak and rose to high frequency. We found that GP-A82V had heightened ability to infect primate cells, including human dendritic cells. The increased infectivity was restricted to cells that have primate-specific NPC1 sequences at the EBOV interface, suggesting that this mutation was indeed an adaptation to the human host. GP-A82V was associated with increased mortality, consistent with the hypothesis that the heightened intrinsic infectivity of GP-A82V contributed to disease severity during the EVD epidemic.

INTRODUCTION

Ebola virus (EBOV) is an enveloped filovirus with a 19-kb, negative-sense, single-stranded RNA genome that causes sporadic outbreaks of lethal hemorrhagic fever in humans (Feldmann and Geisbert, 2011; Kuhn et al., 2010). EBOV was identified as a human pathogen in 1976 (Bowen et al., 1977; Johnson et al., 1977; Pattyn et al., 1977). The high case-fatality rate and self-limited nature of EVD outbreaks suggest that EVD is a zoonosis (Bausch and Schwarz, 2014; Feldmann and Geisbert, 2011). Detection of anti-EBOV antibodies and EBOV RNA in several fruit bat species from central Africa makes them leading candidates for the animal reservoir (Hayman et al., 2012; Leroy et al., 2005; Ng et al., 2015; Pourrut et al., 2007, 2009). Historically, Ebola virus disease (EVD) outbreaks have been geographically limited and resolved after at most a few hundred cases (CDC, 2016). In contrast, the epidemic caused by the EBOV Makona variant was much larger: it began in Guinea in 2013 (Baize et al., 2014), spread to Sierra Leone and Liberia in 2014, and infected more than 28,000 people before it was controlled in 2016 (WHO, 2016).

Although sociological and epidemiological factors were central to the 2013–2016 epidemic's unprecedented scale (Alexander et al., 2015), researchers have also examined the possibility that genetic changes unique to EBOV Makona played a role. To date, experiments with EBOV Makona have not detected evidence for increased replication phenotypes. Studies in primates and in immunodeficient mice, for example, failed to detect increased virulence with EBOV Makona compared to EBOV Mayinga, the 1976 reference isolate (Marzi et al., 2015; Smither et al., 2016). Likewise, the EBOV Makona immunomodulatory proteins VP35 and VP24 inhibited interferon signaling to the same extent as the analogous proteins encoded by EBOV from previous outbreaks (Dunham et al., 2015). These studies, however, examined only the early reference EBOV Makona isolate from Kissidougou, Guinea (C-15), and did not address possible changes in the virus over the course of the epidemic.

The large number of human-to-human transmissions of EBOV Makona during the 2013–2016 EVD epidemic provided greater opportunity for EBOV to adapt to the human host than in any previous outbreak. As expected for an RNA virus, monitoring over the course of the EVD epidemic revealed mutations throughout the genome of EBOV Makona (Carroll et al., 2015; Gire et al., 2014; Simon-Loriere et al., 2015). However, except for the mucin-like domain in the glycoprotein (GP), which is under diversifying selection by the host humoral immune system, most of

the EBOV genome exhibited purifying selection (Park et al., 2015). Although most nonsynonymous mutations detected during the epidemic probably had little effect on viral fitness, it is possible that some of these mutations proliferated because they conferred an advantage to the virus. One such candidate is the clade-defining A82V substitution in EBOV Makona GP, which emerged at a time in the epidemic just before the number of EVD cases increased exponentially. This mutation is particularly intriguing because it is located in the receptor-binding domain of EBOV GP. Here we describe our efforts to determine whether GP-A82V conferred a replication advantage to the virus.

RESULTS

GP-A82V Was First Detected Just Prior to the Exponential Increase in Cases and Rapidly Exceeded the Prevalence of the Ancestral Makona EBOV

To get the broadest possible perspective on the EBOV sequence evolution that took place during the 2013–2016 EVD epidemic, we generated a phylogenetic tree using 1,489 EBOV Makona sequences for which near-complete genomes were available (Tables S1 and S2). The tree demonstrated two distinct lineages (Figure 1A). The first lineage consisted of 86 sequences and was largely confined to the region around Conakry, Guinea. The second lineage formed a monophyletic clade comprised of 1,403 genomes sampled between March 2014 and August 2015. The second lineage included EBOV from all countries affected by the epidemic and was largely defined by two mutations: a non-synonymous C-to-T substitution at nucleotide 6,283, resulting in the GP-A82V substitution, and a synonymous T-to-C substitution at nucleotide 1,849, which encodes amino acid D460 of the viral NP. In addition to being present in the vast majority of EBOV infections during the 2013–2016 epidemic, the GP-A82V mutant was of interest because residue 82 is located at the receptor binding interface (Gong et al., 2016; Wang et al., 2016).

The two lineages were plotted according to date and country of sampling (Figures 1B–1E). GP-A82V was first sampled in Guinea in March 2014. It was next sampled in May 2014 in Sierra Leone. In June 2014 the GP-A82V lineage was again sampled in Guinea. The number of EVD cases caused by GP-A82V in Liberia and Sierra Leone grew rapidly in the summer and fall of 2014 with no apparent contribution from the first, ancestral lineage. In the fall of 2014, EBOV was re-introduced into Guinea from Liberia and Sierra Leone, resulting in a burst of additional cases (Carroll et al., 2015; Quick et al., 2016; Simon-Loriere et al., 2015).

We detected 114 additional amino acid substitutions in the EBOV Makona GP population, though none of these approached the prevalence of GP-A82V. The majority of these were not pursued further because they were located in the mucin-like domain, which is dispensable for entry into target cells (Chandran et al., 2005; Jeffers et al., 2002; Kaletsky et al., 2007; Schornberg et al., 2006). Instead, we focused on a sub-lineage of GP-A82V with an A-to-G change at nucleotide 6,726 that results in a GP-A82V/T230A double mutant (Figure 1A). Aside from GP-A82V, T230A was the most frequently observed non-synonymous mutation (2.5%) outside of the mucin-like domain. Four isolates from the GP-A82V/T230A sub-lineage possessed an additional A-to-G substitution at nucleotide 7,947 that resulted in the triple mutant, GP-A82V/T230A/D637G. These mutants were studied further, as described below.

EBOV Makona GP-A82V Increases Infectivity in Human Cells

The naturally occurring GP mutants A82V, A82V/T230A, and A82V/T230A/D637G were evaluated for their ability to infect cells by placing them in a mammalian expression plasmid containing the gene encoding EBOV Makona GP. Plasmids were constructed for the ancestral sequence and for each mutant combination. Additionally, the single mutants GP-T230A and GP-D637G were constructed, although these mutations were never observed independently of GP-A82V during the epidemic. The expression plasmids were used to generate EBOV GP-pseudotyped lentiviral virion particles bearing a GFP reporter gene. Equal volumes of each supernatant were used to transduce the human osteosarcoma cell line U2OS after confirming that each construct generated comparable amounts of particles by measuring reverse transcriptase activity in the supernatant. 72 hr later, the transduction efficiency for each GP was assessed by measuring the percent GFP-positive cells by flow cytometry. Lentiviruses bearing GP-A82V, GP-A82V/T230A, or GP-A82V/T230A/D637G produced 4-fold more GFP-positive cells than did particles bearing the ancestral GP (Figure 2A). In contrast, pseudotypes bearing either of the single mutants GP-T230A or GP-D637G produced GFP-positive cells at a rate similar to the ancestral GP.

To determine whether the observed infectivity differences were particular to U2OS cells, similar transductions were performed with HEK293 cells as target cells. In HEK293 cells, a 2-fold increase in infectivity was observed with lentiviral particles pseudotyped with GP-A82V, GP-A82V/T230A, or GP-A82V/T230A/D637G (Figure 2B). Once again, no statistically significant changes were observed with transductions using either of the single mutants GP-T230A or GP-D637G.

Dendritic cells (DCs) are targets for EBOV replication in vivo, at both early and later stages of infection (Geisbert et al., 2003). We therefore looked at the effect of the GP mutants on infection of this critical cell type (Figure 2C). Human monocyte-derived DCs were generated from eight blood donors. These cells were challenged with ancestral and with mutant EBOV GP-pseudotyped lentiviral vectors. As compared to the ancestral GP, A82V-containing GPs had significantly enhanced infectivity, while individually the T230A and D637G substitutions either had no effect or had less infectivity.

Amino acid substitutions introduced into the EBOV GP may alter rates of protein production and processing, protein stability, or protein incorporation into virions. To determine whether any of these properties were changed by the EBOV GP mutants, the amount of ancestral versus mutant GP present in our EBOV GP-pseudotyped lentiviruses was compared. EBOV GP-pseudotyped lentiviruses were enriched by acceleration through a 25% sucrose cushion, and virion-associated proteins were analyzed by western blotting, using polyclonal antiserum against a V5 epitope tag that was appended to the carboxyl terminus of the GP. GP is cleaved by furin into two components, GP1 and GP2, and our western blot showed two distinct bands. One

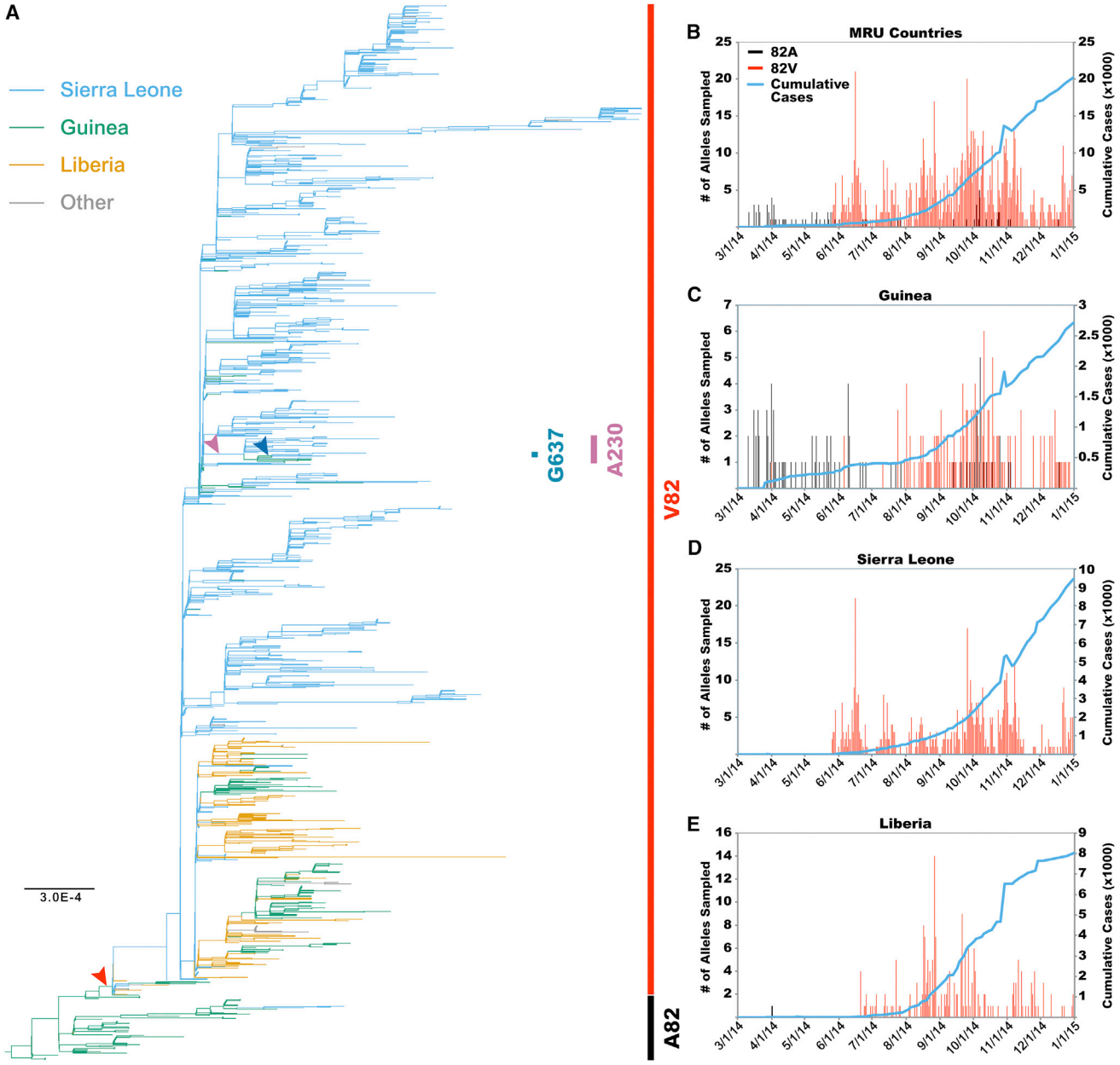

Figure 1. Evolution of GP-A82V Coincides with Dramatic Increase in EBOV Infections

(A) Maximum likelihood phylogeny of 1,489 full-length Makona EBOV sequences. Branches are color coded according to country of sampling. Bars to the right side indicate GP sequence and arrowheads indicate when individual residue changes occurred. Scale bar indicates nucleotide substitutions/site.

(B–E) Plots of the temporal sampling of EBOV GP genotypes during 2014 (left axis) and the cumulative number of EVD cases (right axis). Shown are data for all Mano River Union (MRU) countries (B), Guinea (C), Sierra Leone (D), and Liberia (E).

See also Tables S1 and S2 and Data S1.

band was 70 kDa, consistent in size with full-length GP, either uncleaved by furin or GP1+GP2 covalently bound by disulfide linkages (Figure 2D). The second band was 25 kDa, consistent with the furin-processed GP2 product. GP1 + GP2 band intensity was compared to the intensity of the lentivirion capsid core (p24). All GPs showed equivalent levels of incorporation into particles, indicating that the enhanced infectivity observed in human cells with the GP-A82V-containing EBOV GPs was not due to differences in protein synthesis, processing, or GP incorporation into lentiviral particles.

GP-A82V Enhances GP-Mediated Entry of EBOV Virion Cores into the Target Cell Cytoplasm

The EBOV matrix protein VP40 is sufficient to drive assembly and budding of filamentous virus-like particles (VLPs) from the producer cell plasma membrane (Geisbert and Jahrling, 1995;

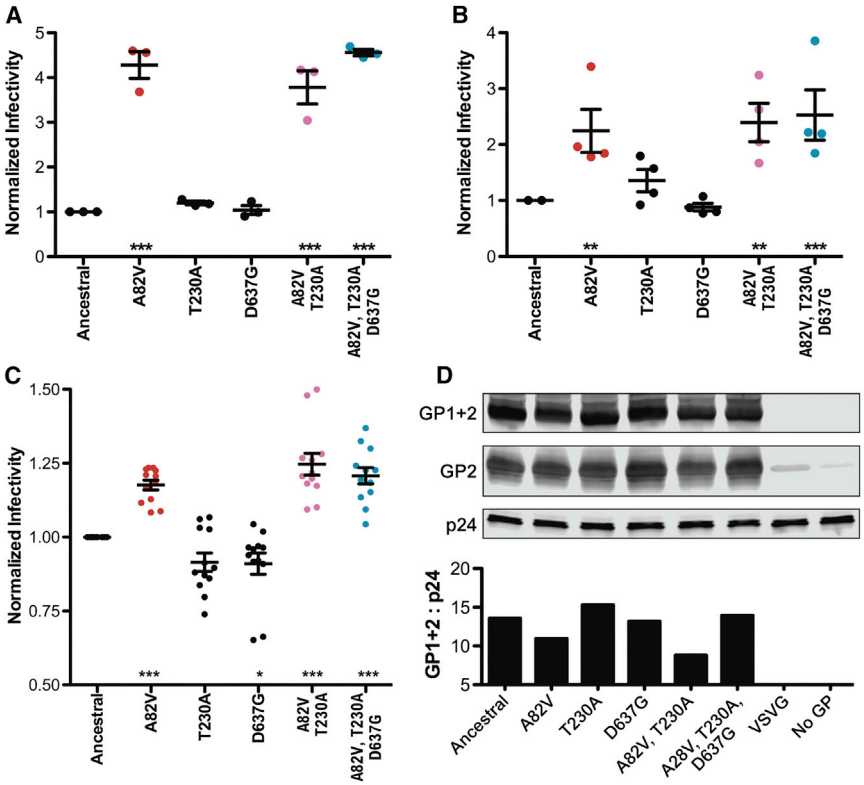

Figure 2. GP-A82V Enhances EBOV Infectivity in Human Cells

(A–C) Lentiviral virions bearing a GFP transgene and pseudotyped with ancestral EBOV Makona GP or the indicated GP variants were produced by transfection of HEK293 cells and used to transduce U2OS cells (A), HEK293 cells (B), or MDDCs (C). GFP-positive cells resulting from transduction with variant GPs were quantified by flow cytometry and normalized to the ancestral GP using lentivirions produced in parallel. Shown are means ± SEM.

(D) Western blots (top) of enriched lentiviral particles pseudotyped with C-terminally V5-tagged EBOV GPs probed with anti-V5 and anti-p24 antibodies. Bar graph showing EBOV GP1 + 2 signal intensity relative to that observed for the corresponding lentiviral capsid (p24).

In (A) and (B), each data point represents a normalized transduction using lentiviral stocks derived from independent transfections. In (C), data points represent independent experiments with four independent viral stocks and eight different human donors. *$p < 0.05$; **$p < 0.001$; ***$p < 0.001$; repeated-measures ANOVA with Dunnett's post-test comparing to ancestral EBOV GP.

Noda et al., 2002). VP40 is also sufficient for incorporation of EBOV GP into the virion membrane, such that the resulting particles are capable of bona fide receptor-mediated entry into target cell cytoplasm. To facilitate quantitation of EBOV GP-mediated entry, EBOV VP40 fused to β-lactamase was used to generate VLPs. These VLPs were used to infect target cells, and subsequently target cells were loaded with a fluorogenic substrate that is trapped within the target cell cytoplasm. The substrate can be cleaved only if the GP successfully attaches, binds, and triggers fusion, releasing β-lactamase-VP40 into the cytoplasm (Manicassamy and Rong, 2009; Tscherne et al., 2010). This experimental system does not require transcription of reporter genes, and therefore more directly tests whether the EBOV GP mutants increase the ability of EBOV VP40 cores to enter into the target cell cytoplasm. β-lactamase-containing VLPs bearing ancestral or mutant EBOV GPs were incubated with U2OS target cells, and then cells were loaded with the fluorogenic substrate. GP-A82V- or GP-A82V/T230A-bearing particles exhibited a significant increase in entry as compared with the ancestral EBOV GP (Figure 3). In contrast, a decrease in entry was measured with the T230A and D637G mutant GPs.

GP-A82V Increases Infectivity in Primate Cells but Not in Cells from Other Species

Next, we determined whether GP-A82V was more infectious for cells of any permissive species or whether the increased infectivity was a human-specific adaptation. NPC1 is the main cellular receptor for EBOV (Carette et al., 2011; Côté et al., 2011), and the EBOV GP-interacting region of NPC1 has been well defined (Gong et al., 2016; Krishnan et al., 2012; Wang et al., 2016). Because the EBOV interacting loop 2 of NPC1 is positioned in close proximity to EBOV GP-82, we assessed species-specific amino acid differences within this portion of NPC1 from 49 mammalian species (Figures 4A and 4B, Table S3).

EBOV interacting loop 2 of NPC1 is almost perfectly conserved in primates (Figure 4B). Only two species, the New World monkey *Callithrix jacchus* and the lemur *Microcebus murinus*, harbor amino acid differences from those found in human NPC1: K499I in *Callithrix jacchus* and K499V in *Microcebus murinus*. Outside of primates, nearly all species have a non-polar amino acid at residue 499, the exception being rabbits (*Oryctolagus cuniculus*), which have a glutamine. Several species harbor amino acid changes in residue 502. Previous studies have shown that a D-to-F substitution at residue 502 disrupts interaction between EBOV GP and NPC1 in straw colored fruit bats (*Eidolon helvum*) (Ng et al., 2015), and it is likely that similar substitutions would prevent EBOV infection in killer whales (*Orcinus orca*), pigs (*Sus scrofa*), Jamaican fruit bats (*Artibeus jamaicensis*), and possibly the common vampire bat (*Desmodus rotundus*).

Based on the NPC1 sequence alignments, we anticipated that infections using EBOV GP-A82V variants in non-human primate cells would result in a similar enhancement to that seen in human cells. To test this prediction, we transduced cells from several primate species, as well as carnivores and rodents, with GFP-expressing lentiviral vectors pseudotyped with the EBOV GPs. Indeed, cells from non-human primates were more susceptible to infection by GP-A82V (Figure 4C). In contrast, cells from rodents and carnivores showed no difference in infectivity between

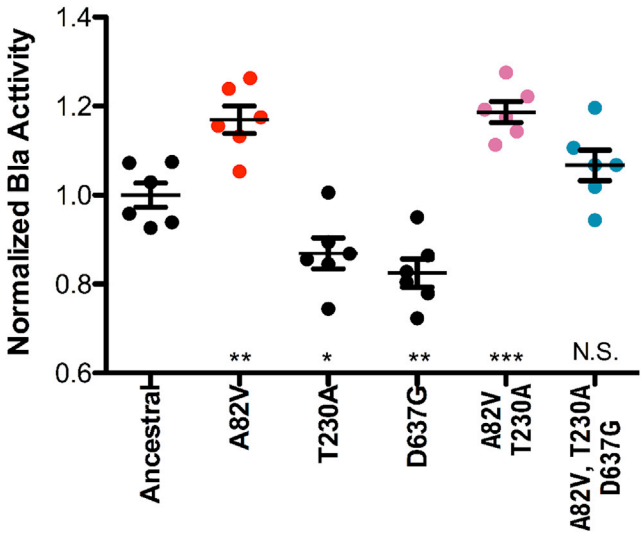

Figure 3. EBOV GP-A82V Enhances the Ability of EBOV Virion Cores to Fuse with Target Cell Cytoplasm

Virus-like particles (VLPs) were generated with EBOV VP40-β-lactamase fusion protein and either the ancestral EBOV GP or one of the indicated mutants. U2OS cells were incubated with VLP-containing supernatant for 2 hr at 4°C, then for 2 hr at 37°C, and then loaded with CCF4-AM overnight at 11°C. Cleavage of CCF4-AM was measured using a fluorescent plate reader with 400/30 excitation and 460/40 emission filters. Signal for cleaved CCF4-AM signal for all EBOV GPs was compared to that observed with the ancestral EBOV GP. Data are means ± SEM (n = 6 viral infections) from a representative experiment. *p < 0.05; **p < 0.01; ***p < 0.001; N.S. p > 0.05; one-way ANOVA with Burnett's post-test comparing with ancestral EBOV GP.

the ancestral EBOV GP and GP-A82V. These results demonstrate that GP-A82V provides primate-specific enhancement of infectivity.

Homology modeling was used to examine how EBOV GP-A82V and NPC1 loop 2 domain orthologs from the mammalian species tested here—as well as from bat species that are potential EBOV reservoirs—may alter virus-host interactions (Figure 5). The EBOV GP-A82V mutation is located on the α1 helix that directly interacts with NPC1 loop 2 (Figure 5A), though residue 82 is located on the back side of the helix. In terms of how V82 is likely to affect the viral GP, our modeling suggests that the GP-A82V mutation will have little impact on the α1 helix backbone itself. Rather, the additional alkane branches in the side chain of valine compared to alanine may differentially impact neighboring amino acids such as the arginine at residue 85 (Figures 5B and 5C). R85 extends into a charged pocket present on the opposite side of the α1 helix to where NPC1 interaction occurs and the nitrogens of the terminal guanidinium group are likely to form ionic interactions with the sidechains of E178, Y109, and the backbone hydroxyl group of A76. On the host side, several amino acid differences in the NPC1 loop 2 domain among mammals are likely to impact filovirus susceptibility in a species-specific manner (Wang et al., 2016; Zhao et al., 2016). Specifically, a lysine is found at residue 499 in primates while all other species examined possess a non-polar residue here and several species, including mouse and dog, possess a tyrosine at 504 in place of phenylalanine (Figures 5D and 5E).

EBOV Makona GP-A82V Is Associated with a Higher Rate of Mortality

To determine whether the GP-A82V mutation had detectable effect on viremia or mortality, we obtained EBOV genotype data from 56 locations in Guinea, Liberia, and Sierra Leone (Arias et al., 2016; Carroll et al., 2015; Gire et al., 2014; Kugelman et al., 2015; Ladner et al., 2015; Park et al., 2015; Quick et al., 2016; Simon-Loriere et al., 2015; Tong et al., 2015) where mortality and viral load information was also available. This data recapitulated the skew (82V > 82A) that was seen in EBOV GP genotype prevalence per country depicted in Figure 1 (Figure 6A). Further analysis was restricted to those cases for which data were available regarding all four parameters: viral load, mortality, sampling location, and viral genotype (Carroll et al., 2015; Gire et al., 2014; Quick et al., 2016). All but 15 of these 194 cases occurred in Guinea, so the analysis was further restricted to Guinea, with samples from 19 districts. After paring down the data, geographic differences in the prevalence of viral genotypes remained (Figure 6B).

We examined associations between viral load (as assessed by C(t) values), risk of death, and GP-82 allele and found that both viral load and possession of GP-A82V were significantly associated with higher mortality. Lower C(t) values (corresponding to higher viral loads) were highly predictive of negative outcome (Figure 6C), consistent with previous reports (de La Vega et al., 2015; Li et al., 2016). GP-A82V-infected individuals had slightly higher viral loads (lower C(t) value, Figure 6D), but the difference was not statistically significant (Student's t test: mean A = 20.07, mean V = 19.68, 95% CI for difference in the means [−0.69, 1.44]; p value = 0.49). Infection by virus with GP-A82V was associated with a significantly higher risk of death (raw odds ratio: 2.64, 95% CI [1.29, 5.38]; Figure 6E).

To better understand the association between GP-A82V and mortality, we modeled the fatality rates for both the ancestral and GP-A82V genotypes over a range of viral loads (transformed C(t) values) (Figure 6F). After correcting for differences in C(t) values, the adjusted odds ratio for GP-A82V remained above 1, but with a wide confidence interval (OR = 2.09, 95% CI [0.94, 4.64]). When we added multiple potential confounding factors, including geographic variation in base fatality rate and access to health care, to the model, they had little effect on the conclusion. We found only modest evidence of geographic variation (Figure S1), while including the cumulative number of EVD cases per region (a proxy for EVD-associated burdens on the health care infrastructure) failed to improve model fit (Figure S1). Taken together, these data suggest an increased risk of death in people infected with GP-A82V, but we cannot rule out that there is no independent effect of the mutation or demonstrate that the association is causal.

DISCUSSION

The devastating 2013–2016 EVD epidemic led to two orders of magnitude more cases than in previous EVD outbreaks (CDC, 2016), providing greater opportunity for EBOV to undergo human adaptive changes than ever before. The A82V mutation in EBOV Makona GP arose early during the outbreak, nearly replacing the ancestral genotype, and was present in the viruses responsible

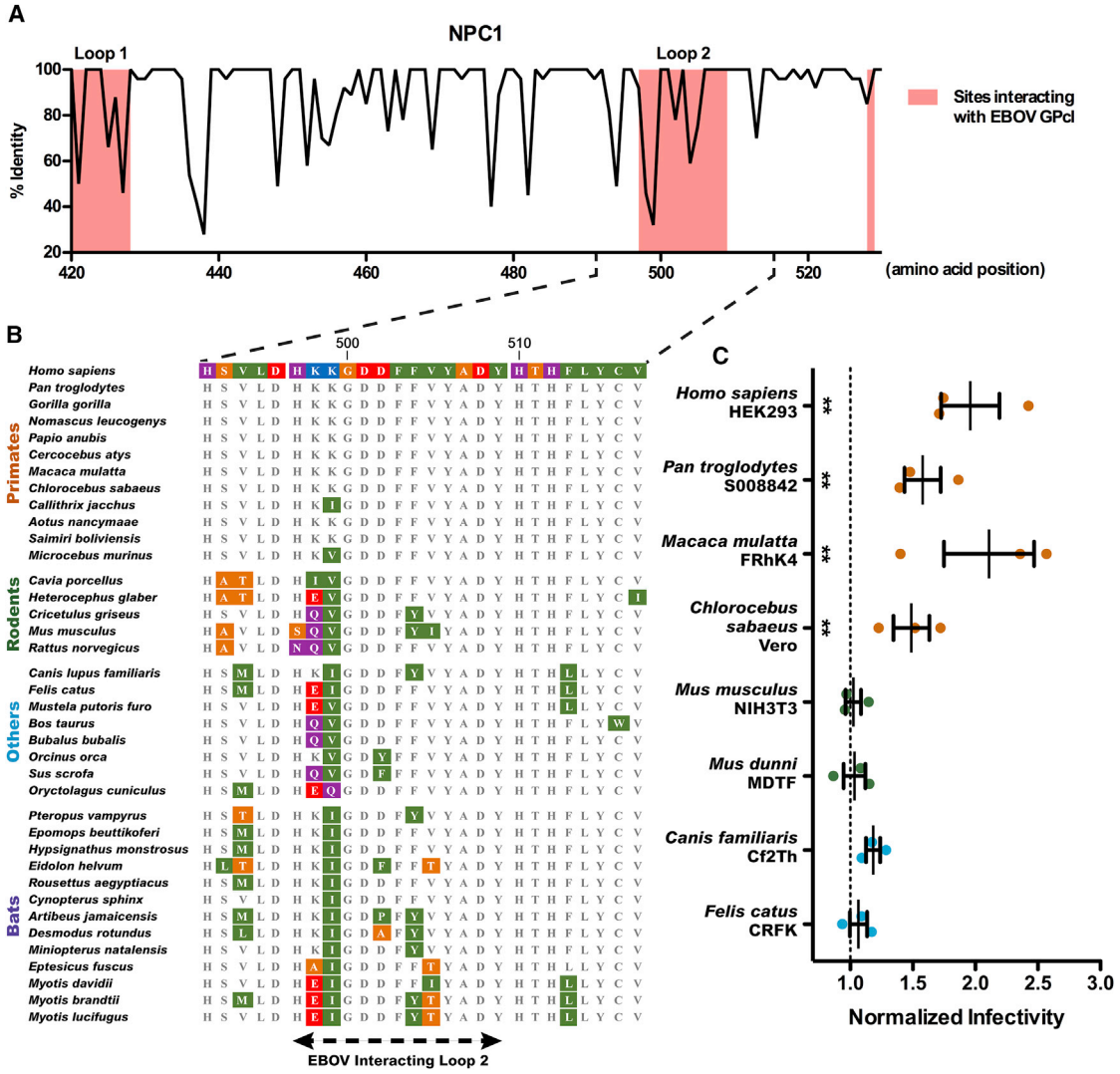

Figure 4. GP-A82V Substitution Specifically Enhances Infectivity in Primate Cells

(A) Plot of the amino acid conservation in mammals across the region of NPC1 that interacts with EBOV GP. Shaded regions indicate EBOV-interacting residues of NPC1.

(B) Alignment of NPC1 sequences in and around the second NPC1 interacting loop from a subset of mammalian species used for (A).

(C) Relative infectivity data for EBOV GP containing the A82V substitution in relation to the ancestral GP in four primate cell lines and five cell lines from other mammalian species.

Data are means ± SEM (n = 3), with data points representing infections using independent viral stocks. **$p < 0.01$; repeated-measures ANOVA with Dunnett's post-test comparing to ancestral EBOV GP. See also Table S3.

for the majority of EVD cases during the epidemic (Figure 1). Our data show that GP-A82V enhances infectivity in human and other primate cells but not in cells of other mammalian species (Figures 2 and4). Given that GP-A82V is located at the NPC1 binding interface, we are left with a strong suspicion that GP-A82V represents an EBOV adaptation to the human host. Human population data reveal a modest trend toward higher viremia with GP-A82V and a significant association with increased mortality (Figure 6), raising the intriguing possibility that these phenotypes result from this mutation.

In a co-submitted manuscript, Urbanowicz and colleagues independently arrived at the conclusion that GP-A82V enhances viral infectivity in human cells (Urbanowicz et al., 2016). In their hands, GP-A82V enhanced infectivity within the context of numerous GP sequences observed during the outbreak. Complementary to our findings, they showed that GP-A82V has decreased infectivity for a variety of bat cell lines, species with amino acid substitutions in NPC1 binding loop 2 that are similar to those in the non-primate species tested here (Figures 4 and5). Their data support the hypothesis that A82V is a primate-specific adaptation.

For GP-A82V, our molecular data warrant follow-up with in vivo, high-containment (BSL-4) experiments. Reverse genetics systems have been used to study live EBOV variants

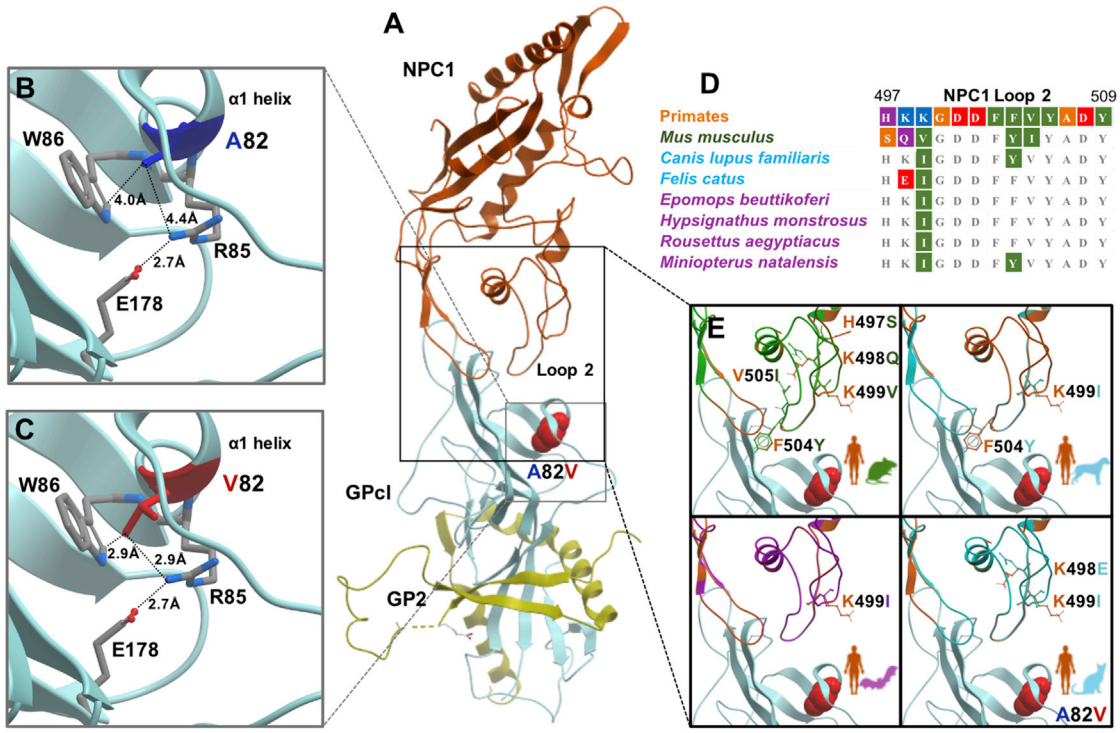

Figure 5. Comparative Structural Analysis of the EBOV GP-A82V Substitution and NPC1 Orthologs

(A) Structural overview of EBOV GP2 (yellow) and cleaved GP (GPcl, light blue) bound to human NPC1 (orange), as experimentally derived by Wang et al. (2016). The EBOV GP-A82V substitution (red) occurs in the α1 helix of proteolytically cleaved GP that interacts with NPC1 loop 2.

(B and C) Zoom of the (B) ancestral GP-A82 (blue) and (C) derived GP-V82 (red) variants in relation to proximal amino acid side chains. The distance between R85 and E178 is close enough (i.e., <4 Å) where a salt bridge is possible.

(D and E) NPC1 loop 2 amino acid (D) sequence alignments and (E) target-template homology models of cell species used in this study (rodents, green; other mammals, cyan; Figure 4) and bats (purple) compared to primates (orange). Highlighted in (C) are the amino acid differences in loop 2 from the target species compared to the template, humans, and their location compared to the GP-A82V variant.

(Volchkov et al., 2001) and can be used for head-to-head comparison of variants in cell culture-based assays (Albariño et al., 2016). Moreover, although human clinical data shows that GP-A82V was associated with higher case fatality rate, controlled BSL-4 experiments could test whether GP-A82V is causal for this clinical phenotype or with higher viral load in non-human primates.

The GP-A82V mutation enhances infectivity for human cells through GP-mediated fusion (Figure 3), suggesting a biologically plausible mechanism for cross-species viral adaptation. Emergence of human viral disease from a reservoir host is a major route of virus transmission, as has been documented for human immunodeficiency viruses type 1 and 2 (HIV-1 and HIV-2), severe acute respiratory virus coronavirus (SARS-CoV), influenza virus, dengue virus, Nipah virus, Hendra virus, and Marburg virus (Parrish et al., 2008). Because of shared co-evolutionary history, zoonotic viruses are thought to replicate and transmit more efficiently in their reservoir hosts than in humans. In a new host, although productive infection may occur, differences in key host factors between cells of the reservoir versus those of the new host can impair important events such as receptor binding and entry, replication of the viral genome, virion assembly and release, and avoidance of the host innate or adaptive immune response. More efficient receptor utilization in the new host is a common route of adaptation and has been described for SARS CoV (Li et al., 2005) and numerous influenza strains (Herfst et al., 2012; Imai et al., 2012; Matrosovich et al., 2000; Stevens et al., 2006a, 2006b; Xu et al., 2010). These experimental findings involving influenza have allowed for more informed surveillance of the animal reservoirs as well as providing a better understanding of the ongoing viral evolution in humans (Dugan et al., 2008; Holmes et al., 2005; Nelson et al., 2008; Obenauer et al., 2006; Rambaut et al., 2008; Russell et al., 2012). The knowledge that EBOV GP mutations that modulate fusion to host cells may be a route for human adaptation, and which GP residues mediate this adaptation is potentially valuable knowledge for surveillance activities during future EBOV epidemics.

The GP-A82V mutation is on the backside of the α1 helix that interacts with NPC1 and is therefore predicted to have little direct impact on binding to NPC1. However, there are likely to be differences in how the alanine and valine side chains pack against neighboring amino acids. Valine contains more alkane branches than alanine, which would place the side chain in closer proximity to GP-R85 and -W86. Steric hindrance between V82 and R85 may alter a predicted salt bridge between R85 and E178 (~2.7 Å apart, Figure 5). In addition, the added

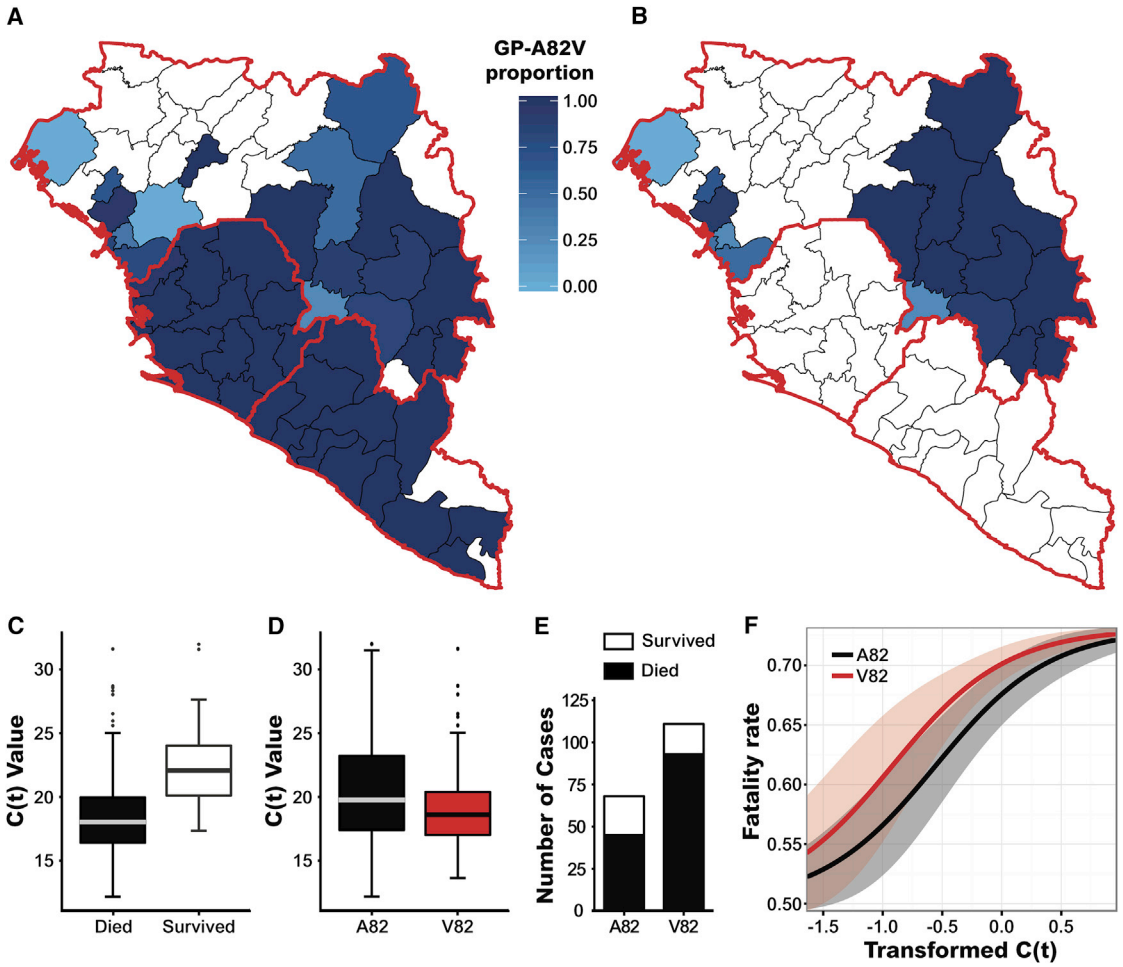

Figure 6. Association between GP-A82V and Increased Rate of Lethal Infection

(A and B) Spatial distribution of GP genotypes for all available EBOV Makona sequencing data (A) or Guinean isolates linked to information regarding clinical outcome and viral load (B). The data included in (B) were used in subsequent modeling analyses.

(C) Association between patient viral load (as determined by C(t) values) and EVD-associated mortality. This analysis used all observations for which C(t) values were measured (n = 313).

(D) Viral load information (as determined by C(t) values) in individuals infected with EBOV encoding either ancestral or A82V GP. This analysis used all observations for which C(t) values were measured (A82: n = 97; V82: n = 216).

Plots in (C) and (D) show mean with the box covering from the second to third quartile (25%–75%) of samples, and the bars marking the 5% and 95% quantiles. Dots represent samples outside of the 95% probability region.

(E) Mortality data in individuals infected with EBOV encoding either ancestral or A82V GP.

(F) Depiction of the correlation between GP genotype and mortality, based on results of a binomial generalized linear model using C(t) values and GP genotype as covariates to predict case fatality rates over a range of viral loads (depicted by transformed C(t) values). C(t) values were transformed by subtracting the mean, dividing by two standard deviations and flipping the sign such that the value 0 in the graph corresponds to the average C(t) value and the transformed variable reflects viral load.

See also Figure S1.

"bulk" of the GP-A82V mutation may alter the α1 helix conformation, to provide better access for proximal resides, such as GP-V79, -P80, -T83, and -W86, to interact with NPC1 (Wang et al., 2016). Compared to the human NPC1 loop 2 domain, the inclusion of hydrophobic side chains at site 499 (valine or isoleucine) in other mammals (non-primates) probably adds more bulk near the backbone, potentially restricting how the loop can adapt to new conformations. Primates also possess a phenylalanine at amino acid 504, while several other species have a tyrosine. Changes between phenylalanine and tyrosine are common, differing only by an ortho hydrogen (phenylalanine) or hydroxyl group (tyrosine) on the benzene ring, and both are generally non-reactive and rarely involved in protein function. F504, however, is predicted to make contact with up to eight residues on EBOV GP (measured by a distance of <4.5 Å [Wang et al., 2016]) and is potentially a critical site for filovirus susceptibility (Zhao et al., 2016). In addition to the effects the A82V substitution could impart to NPC1/GP interactions, it may also alter the

propensity for EBOV GP to undergo "triggering" upon interaction with NPC1. In this context, the triggering process refers to the dramatic conformational changes undertaken by the EBOV GP resulting in the exposure of the viral fusion peptide on GP2, which is normally sequestered by GP1.

If GP-A82V is an adaptation to humans, it remains an open question whether this change led not only to increased replication in human hosts, but also to increased transmission between humans. The GP-A82V mutation was first sampled on March 31, 2014 (Data S1), after only approximately 110 EVD cases (CDC, 2016). Our data show that GP-A82V increases infectivity of EBOV for a variety of human cells in tissue culture and is associated with increased mortality in humans. Although significant questions remain, our findings raise the possibility that this mutation contributed directly to greater transmission and thus to the severity of the outbreak. It is difficult to draw any conclusion about this hypothesis, though, since the frequency increase can also be attributed to stochastic effects, including founder effects as EBOV moved from Guinea into Sierra Leone and multiple re-introductions of GP-A82V back into Guinea. In any case, the early emergence of GP-A82V highlights the need for vigorous surveillance and rapid public health intervention after identification of EVD and other emerging infectious diseases, in order to limit the possibility of viral adaptation to humans. Finally, studies such as this are necessary, as they provide vital biological information crucial for the interpretation of viral sequence evolution. Having this connection between viral genotype and phenotype maximizes the utility of viral sequencing efforts during outbreaks, allowing more efficient targeting of intervention strategies.

STAR★METHODS

Detailed methods are provided in the online version of this paper and include the following:

- KEY RESOURCES TABLE
- CONTACT FOR REAGENT AND RESOURCE SHARING
- EXPERIMENTAL MODELS AND SUBJECT DETAILS
  - Cell Lines and Primary Human MDDCs
- METHOD DETAILS
  - Sequence Data and Alignments
  - Phylogenetic Analysis
  - Cell Culture
  - Plasmid DNA
  - Reporter Virus and Virus-like Particle Production
  - Virus Infectivity Assays
  - Infectivity Assay Using EBOV Virion Cores
  - Analysis of Clinical Data
  - Western Blots
  - Protein Structure Modeling
- QUANTIFICATION AND STATISTICAL ANALYSIS

SUPPLEMENTAL INFORMATION

Supplemental Information includes one figure, three tables, and one data file and can be found with this article online at http://dx.doi.org/10.1016/j.cell.2016.10.014.

AUTHOR CONTRIBUTIONS

W.E.D., A.E.L., A.R., M.G., K.G.A., P.C.S., and J.L. designed and supervised the study. W.E.D., A.E.L., N.D.G., L.M.C., K.K., P.P.K., S.M.M., S.F.S., E.D., A.K., P.M., M.G., and K.G.A. conducted the experiments and collected the datasets. All authors analyzed the data and wrote the manuscript.

ACKNOWLEDGMENTS

We wish to thank Andrew Orry for assistance with the homology modeling and Greg Towers for MDTF cells. This work was supported by NIH grants NIDA DP1DA034990 and NIAID R01AI111809 to J.L., NHGRI 1U01HG007910 to M.G. and J.L., 5T32AI007244-33 to N.D.G., NCATS UL1TR001114 and NIAID HHSN272201400048C to K.G.A., Howard Hughes Medical Investigator award and NIAID U19AI110818 to P.C.S., and European Union Seventh Framework Programme [FP7/2007-2013] Grant No 278433-PREDEMICS to A.R. This material is based upon work supported by the National Science Foundation under grant no. DGE 1144152 (A.E.L.). Some reagents were constructed from NIH grant U19AI110818 (P.C.S.). K.G.A. is a PEW Biomedical Scholar.

Received: August 12, 2016
Revised: September 23, 2016
Accepted: October 6, 2016
Published: November 3, 2016

REFERENCES

Abagyan, R., Totrov, M., and Kuznetsov, D. (1994). ICM—A new method for protein modeling and design: Applications to docking and structure prediction from the distorted native conformation. J. Comput. Chem. *15*, 488–506.

Albariño, C.G., Guerrero, L.W., Chakrabarti, A.K., Kainulainen, M.H., Whitmer, S.L.M., Welch, S.R., and Nichol, S.T. (2016). Virus fitness differences observed between two naturally occurring isolates of Ebola virus Makona variant using a reverse genetics approach. Virology *496*, 237–243.

Alexander, K.A., Sanderson, C.E., Marathe, M., Lewis, B.L., Rivers, C.M., Shaman, J., Drake, J.M., Lofgren, E., Dato, V.M., Eisenberg, M.C., and Eubank, S. (2015). What factors might have led to the emergence of Ebola in West Africa? PLoS Negl. Trop. Dis. *9*, e0003652.

Arias, A., Watson, S.J., Asogun, D., Tobin, E.A., Lu, J., Phan, M.V.T., Jah, U., Wadoum, R.E.G., Meredith, L., Thorne, L., et al. (2016). Rapid outbreak sequencing of Ebola virus in Sierra Leone identifies transmission chains linked to sporadic cases. Virus Evolution *2*, vew16.

Baize, S., Pannetier, D., Oestereich, L., Rieger, T., Koivogui, L., Magassouba, N., Soropogui, B., Sow, M.S., Keïta, S., De Clerck, H., et al. (2014). Emergence of Zaire Ebola virus disease in Guinea. N. Engl. J. Med. *371*, 1418–1425.

Bates, D., Mächler, M., Bolker, B., and Walker, S. (2015). Fitting linear mixed-effects models using lme4. J. Stat. Softw. *67*, 1–48.

Bausch, D.G., and Schwarz, L. (2014). Outbreak of ebola virus disease in Guinea: where ecology meets economy. PLoS Negl. Trop. Dis. *8*, e3056.

Berthoux, L., Sebastian, S., Sokolskaja, E., and Luban, J. (2005). Cyclophilin A is required for TRIM5alpha-mediated resistance to HIV-1 in Old World monkey cells. Proc. Natl. Acad. Sci. USA *102*, 14849–14853.

Bivand, R., and Lewin-Koh, N. (2016). Tools for Reading and Handling Spatial Objects [R package maptools version 0.8-39] (Comprehensive R Archive Network [CRAN]). http://r-forge.r-project.org/projects/maptools/.

Bowen, E.T., Lloyd, G., Harris, W.J., Platt, G.S., Baskerville, A., and Vella, E.E. (1977). Viral haemorrhagic fever in southern Sudan and northern Zaire. Preliminary studies on the aetiological agent. Lancet *1*, 571–573.

Capella-Gutiérrez, S., Silla-Martínez, J.M., and Gabaldón, T. (2009). trimAl: a tool for automated alignment trimming in large-scale phylogenetic analyses. Bioinformatics *25*, 1972–1973.

Carette, J.E., Raaben, M., Wong, A.C., Herbert, A.S., Obernosterer, G., Mulherkar, N., Kuehne, A.I., Kranzusch, P.J., Griffin, A.M., Ruthel, G., et al.

(2011). Ebola virus entry requires the cholesterol transporter Niemann-Pick C1. Nature *477*, 340–343.

Carroll, M.W., Matthews, D.A., Hiscox, J.A., Elmore, M.J., Pollakis, G., Rambaut, A., Hewson, R., García-Dorival, I., Bore, J.A., Koundouno, R., et al. (2015). Temporal and spatial analysis of the 2014-2015 Ebola virus outbreak in West Africa. Nature *524*, 97–101.

CDC (2016). Outbreaks Chronology: Ebola Virus Disease | Ebola Hemorrhagic Fever | CDC. http://www.cdc.gov/vhf/ebola/outbreaks/history/chronology.html (CDC).

Chandran, K., Sullivan, N.J., Felbor, U., Whelan, S.P., and Cunningham, J.M. (2005). Endosomal proteolysis of the Ebola virus glycoprotein is necessary for infection. Science *308*, 1643–1645.

Chesebro, B., Wehrly, K., Nishio, J., and Perryman, S. (1992). Macrophage-tropic human immunodeficiency virus isolates from different patients exhibit unusual V3 envelope sequence homogeneity in comparison with T-cell-tropic isolates: definition of critical amino acids involved in cell tropism. J. Virol. *66*, 6547–6554.

Côté, M., Misasi, J., Ren, T., Bruchez, A., Lee, K., Filone, C.M., Hensley, L., Li, Q., Ory, D., Chandran, K., and Cunningham, J. (2011). Small molecule inhibitors reveal Niemann-Pick C1 is essential for Ebola virus infection. Nature *477*, 344–348.

de La Vega, M.-A., Caleo, G., Audet, J., Qiu, X., Kozak, R.A., Brooks, J.I., Kern, S., Wolz, A., Sprecher, A., Greig, J., et al. (2015). Ebola viral load at diagnosis associates with patient outcome and outbreak evolution. J. Clin. Invest. *125*, 4421–4428.

Diehl, W.E., Stansell, E., Kaiser, S.M., Emerman, M., and Hunter, E. (2008). Identification of postentry restrictions to Mason-Pfizer monkey virus infection in New World monkey cells. J. Virol. *82*, 11140–11151.

Dugan, V.G., Chen, R., Spiro, D.J., Sengamalay, N., Zaborsky, J., Ghedin, E., Nolting, J., Swayne, D.E., Runstadler, J.A., Happ, G.M., et al. (2008). The evolutionary genetics and emergence of avian influenza viruses in wild birds. PLoS Pathog. *4*, e1000076.

Dunham, E.C., Banadyga, L., Groseth, A., Chiramel, A.I., Best, S.M., Ebihara, H., Feldmann, H., and Hoenen, T. (2015). Assessing the contribution of interferon antagonism to the virulence of West African Ebola viruses. Nat. Commun. *6*, 8000.

Feldmann, H., and Geisbert, T.W. (2011). Ebola haemorrhagic fever. Lancet *377*, 849–862.

Geisbert, T.W., and Jahrling, P.B. (1995). Differentiation of filoviruses by electron microscopy. Virus Res. *39*, 129–150.

Geisbert, T.W., Hensley, L.E., Larsen, T., Young, H.A., Reed, D.S., Geisbert, J.B., Scott, D.P., Kagan, E., Jahrling, P.B., and Davis, K.J. (2003). Pathogenesis of Ebola hemorrhagic fever in cynomolgus macaques: evidence that dendritic cells are early and sustained targets of infection. Am. J. Pathol. *163*, 2347–2370.

Gelman, A. (2008). Scaling regression inputs by dividing by two standard deviations. Stat. Med. *27*, 2865–2873.

Gire, S.K., Goba, A., Andersen, K.G., Sealfon, R.S.G., Park, D.J., Kanneh, L., Jalloh, S., Momoh, M., Fullah, M., Dudas, G., et al. (2014). Genomic surveillance elucidates Ebola virus origin and transmission during the 2014 outbreak. Science *345*, 1369–1372.

Gong, X., Qian, H., Zhou, X., Wu, J., Wan, T., Cao, P., Huang, W., Zhao, X., Wang, X., Wang, P., et al. (2016). Structural insights into the Niemann-Pick C1 (NPC1)-mediated cholesterol transfer and Ebola infection. Cell *165*, 1467–1478.

Hayman, D.T.S., Yu, M., Crameri, G., Wang, L.-F., Suu-Ire, R., Wood, J.L.N., and Cunningham, A.A. (2012). Ebola virus antibodies in fruit bats, Ghana, West Africa. Emerg. Infect. Dis. *18*, 1207–1209.

Herfst, S., Schrauwen, E.J.A., Linster, M., Chutinimitkul, S., de Wit, E., Munster, V.J., Sorrell, E.M., Bestebroer, T.M., Burke, D.F., Smith, D.J., et al. (2012). Airborne transmission of influenza A/H5N1 virus between ferrets. Science *336*, 1534–1541.

Holmes, E.C., Ghedin, E., Miller, N., Taylor, J., Bao, Y., St George, K., Grenfell, B.T., Salzberg, S.L., Fraser, C.M., Lipman, D.J., and Taubenberger, J.K. (2005). Whole-genome analysis of human influenza A virus reveals multiple persistent lineages and reassortment among recent H3N2 viruses. PLoS Biol. *3*, e300.

Imai, M., Watanabe, T., Hatta, M., Das, S.C., Ozawa, M., Shinya, K., Zhong, G., Hanson, A., Katsura, H., Watanabe, S., et al. (2012). Experimental adaptation of an influenza H5 HA confers respiratory droplet transmission to a reassortant H5 HA/H1N1 virus in ferrets. Nature *486*, 420–428.

Jeffers, S.A., Sanders, D.A., and Sanchez, A. (2002). Covalent modifications of the ebola virus glycoprotein. J. Virol. *76*, 12463–12472.

Johnson, K.M., Lange, J.V., Webb, P.A., and Murphy, F.A. (1977). Isolation and partial characterisation of a new virus causing acute haemorrhagic fever in Zaire. Lancet *1*, 569–571.

Kaletsky, R.L., Simmons, G., and Bates, P. (2007). Proteolysis of the Ebola virus glycoproteins enhances virus binding and infectivity. J. Virol. *81*, 13378–13384.

Katoh, K., and Standley, D.M. (2013). MAFFT multiple sequence alignment software version 7: improvements in performance and usability. Mol. Biol. Evol. *30*, 772–780.

Krishnan, A., Miller, E.H., Herbert, A.S., Ng, M., Ndungo, E., Whelan, S.P., Dye, J.M., and Chandran, K. (2012). Niemann-Pick C1 (NPC1)/NPC1-like1 chimeras define sequences critical for NPC1's function as a flovirus entry receptor. Viruses *4*, 2471–2484.

Kugelman, J.R., Wiley, M.R., Mate, S., Ladner, J.T., Beitzel, B., Fakoli, L., Taweh, F., Prieto, K., Diclaro, J.W., Minogue, T., et al.; US Army Medical Research Institute of Infectious Diseases; National Institutes of Health; Integrated Research Facility–Frederick Ebola Response Team 2014–2015 (2015). Monitoring of Ebola virus Makona evolution through establishment of advanced genomic capability in Liberia. Emerg. Infect. Dis. *21*, 1135–1143.

Kuhn, J.H., Becker, S., Ebihara, H., Geisbert, T.W., Johnson, K.M., Kawaoka, Y., Lipkin, W.I., Negredo, A.I., Netesov, S.V., Nichol, S.T., et al. (2010). Proposal for a revised taxonomy of the family Filoviridae: classification, names of taxa and viruses, and virus abbreviations. Arch. Virol. *155*, 2083–2103.

Ladner, J.T., Wiley, M.R., Mate, S., Dudas, G., Prieto, K., Lovett, S., Nagle, E.R., Beitzel, B., Gilbert, M.L., Fakoli, L., et al. (2015). Evolution and spread of Ebola virus in Liberia, 2014-2015. Cell Host Microbe *18*, 659–669.

Laguette, N., Sobhian, B., Casartelli, N., Ringeard, M., Chable-Bessia, C., Ségéral, E., Yatim, A., Emiliani, S., Schwartz, O., and Benkirane, M. (2011). SAMHD1 is the dendritic- and myeloid-cell-specific HIV-1 restriction factor counteracted by Vpx. Nature *474*, 654–657.

Leroy, E.M., Kumulungui, B., Pourrut, X., Rouquet, P., Hassanin, A., Yaba, P., Délicat, A., Paweska, J.T., Gonzalez, J.-P., and Swanepoel, R. (2005). Fruit bats as reservoirs of Ebola virus. Nature *438*, 575–576.

Li, W., Zhang, C., Sui, J., Kuhn, J.H., Moore, M.J., Luo, S., Wong, S.-K., Huang, I.-C., Xu, K., Vasilieva, N., et al. (2005). Receptor and viral determinants of SARS-coronavirus adaptation to human ACE2. EMBO J. *24*, 1634–1643.

Li, J., Duan, H.-J., Chen, H.-Y., Ji, Y.-J., Zhang, X., Rong, Y.-H., Xu, Z., Sun, L.-J., Zhang, J.-Y., Liu, L.-M., et al. (2016). Age and Ebola viral load correlate with mortality and survival time in 288 Ebola virus disease patients. Int. J. Infect. Dis. *42*, 34–39.

Manicassamy, B., and Rong, L. (2009). Expression of Ebolavirus glycoprotein on the target cells enhances viral entry. Virol. J. *6*, 75.

Marzi, A., Feldmann, F., Hanley, P.W., Scott, D.P., Günther, S., and Feldmann, H. (2015). Delayed disease progression in cynomolgus macaques infected with Ebola virus Makona strain. Emerg. Infect. Dis. *21*, 1777–1783.

Matrosovich, M., Tuzikov, A., Bovin, N., Gambaryan, A., Klimov, A., Castrucci, M.R., Donatelli, I., and Kawaoka, Y. (2000). Early alterations of the receptor-binding properties of H1, H2, and H3 avian influenza virus hemagglutinins after their introduction into mammals. J. Virol. *74*, 8502–8512.

Nègre, D., Mangeot, P.E., Duisit, G., Blanchard, S., Vidalain, P.O., Leissner, P., Winter, A.J., Rabourdin-Combe, C., Mehtali, M., Moullier, P., et al. (2000). Characterization of novel safe lentiviral vectors derived from simian

immunodeficiency virus (SIVmac251) that efficiently transduce mature human dendritic cells. Gene Ther. *7*, 1613–1623.

Nelson, M.I., Viboud, C., Simonsen, L., Bennett, R.T., Griesemer, S.B., St George, K., Taylor, J., Spiro, D.J., Sengamalay, N.A., Ghedin, E., et al. (2008). Multiple reassortment events in the evolutionary history of H1N1 influenza A virus since 1918. PLoS Pathog. *4*, e1000012.

Ng, M., Ndungo, E., Kaczmarek, M.E., Herbert, A.S., Binger, T., Kuehne, A.I., Jangra, R.K., Hawkins, J.A., Gifford, R.J., Biswas, R., et al. (2015). Filovirus receptor NPC1 contributes to species-specific patterns of ebolavirus susceptibility in bats. eLife *4*, 4.

Noda, T., Sagara, H., Suzuki, E., Takada, A., Kida, H., and Kawaoka, Y. (2002). Ebola virus VP40 drives the formation of virus-like filamentous particles along with GP. J. Virol. *76*, 4855–4865.

Obenauer, J.C., Denson, J., Mehta, P.K., Su, X., Mukatira, S., Finkelstein, D.B., Xu, X., Wang, J., Ma, J., Fan, Y., et al. (2006). Large-scale sequence analysis of avian influenza isolates. Science *311*, 1576–1580.

Park, D.J., Dudas, G., Wohl, S., Goba, A., Whitmer, S.L.M., Andersen, K.G., Sealfon, R.S., Ladner, J.T., Kugelman, J.R., Matranga, C.B., et al. (2015). Ebola virus epidemiology, transmission, and evolution during seven months in Sierra Leone. Cell *161*, 1516–1526.

Parrish, C.R., Holmes, E.C., Morens, D.M., Park, E.-C., Burke, D.S., Calisher, C.H., Laughlin, C.A., Saif, L.J., and Daszak, P. (2008). Cross-species virus transmission and the emergence of new epidemic diseases. Microbiol. Mol. Biol. Rev. *72*, 457–470.

Pattyn, S., van der Groen, G., Jacob, W., Piot, P., and Courteille, G. (1977). Isolation of Marburg-like virus from a case of haemorrhagic fever in Zaire. Lancet *1*, 573–574.

Pickett, B.E., Sadat, E.L., Zhang, Y., Noronha, J.M., Squires, R.B., Hunt, V., Liu, M., Kumar, S., Zaremba, S., Gu, Z., et al. (2012). ViPR: an open bioinformatics database and analysis resource for virology research. Nucleic Acids Res. *40*, D593–D598.

Pourrut, X., Délicat, A., Rollin, P.E., Ksiazek, T.G., Gonzalez, J.-P., and Leroy, E.M. (2007). Spatial and temporal patterns of Zaire ebolavirus antibody prevalence in the possible reservoir bat species. J. Infect. Dis. *196* (*Suppl 2*), S176–S183.

Pourrut, X., Souris, M., Towner, J.S., Rollin, P.E., Nichol, S.T., Gonzalez, J.-P., and Leroy, E. (2009). Large serological survey showing cocirculation of Ebola and Marburg viruses in Gabonese bat populations, and a high seroprevalence of both viruses in *Rousettus aegyptiacus*. BMC Infect. Dis. *9*, 159.

Quick, J., Loman, N.J., Duraffour, S., Simpson, J.T., Severi, E., Cowley, L., Bore, J.A., Koundouno, R., Dudas, G., Mikhail, A., et al. (2016). Real-time, portable genome sequencing for Ebola surveillance. Nature *530*, 228–232.

R Core Team (2016). R: A Language and Environment for Statistical Computing.

Rambaut, A., Pybus, O.G., Nelson, M.I., Viboud, C., Taubenberger, J.K., and Holmes, E.C. (2008). The genomic and epidemiological dynamics of human influenza A virus. Nature *453*, 615–619.

Reinhard, C., Bottinelli, D., Kim, B., and Luban, J. (2014). Vpx rescue of HIV-1 from the antiviral state in mature dendritic cells is independent of the intracellular deoxynucleotide concentration. Retrovirology *11*, 12.

Russell, C.A., Fonville, J.M., Brown, A.E.X., Burke, D.F., Smith, D.L., James, S.L., Herfst, S., van Boheemen, S., Linster, M., Schrauwen, E.J., et al. (2012). The potential for respiratory droplet-transmissible A/H5N1 influenza virus to evolve in a mammalian host. Science *336*, 1541–1547.

Sanchez, A., Trappier, S.G., Mahy, B.W., Peters, C.J., and Nichol, S.T. (1996). The virion glycoproteins of Ebola viruses are encoded in two reading frames and are expressed through transcriptional editing. Proc. Natl. Acad. Sci. USA *93*, 3602–3607.

Schornberg, K., Matsuyama, S., Kabsch, K., Delos, S., Bouton, A., and White, J. (2006). Role of endosomal cathepsins in entry mediated by the Ebola virus glycoprotein. J. Virol. *80*, 4174–4178.

Simon-Loriere, E., Faye, O., Faye, O., Koivogui, L., Magassouba, N., Keita, S., Thiberge, J.-M., Diancourt, L., Bouchier, C., Vandenbogaert, M., et al. (2015). Distinct lineages of Ebola virus in Guinea during the 2014 West African epidemic. Nature *524*, 102–104.

Smither, S.J., Eastaugh, L., Ngugi, S., O'Brien, L., Phelps, A., Steward, J., and Lever, M.S. (2016). Ebola virus Makona shows reduced lethality in an immune-deficient mouse model. J. Infect. Dis. *214* (*Suppl 3*), S268–S274.

Stamatakis, A., Ludwig, T., and Meier, H. (2005). RAxML-III: a fast program for maximum likelihood-based inference of large phylogenetic trees. Bioinformatics *21*, 456–463.

Stevens, J., Blixt, O., Glaser, L., Taubenberger, J.K., Palese, P., Paulson, J.C., and Wilson, I.A. (2006a). Glycan microarray analysis of the hemagglutinins from modern and pandemic influenza viruses reveals different receptor specificities. J. Mol. Biol. *355*, 1143–1155.

Stevens, J., Blixt, O., Tumpey, T.M., Taubenberger, J.K., Paulson, J.C., and Wilson, I.A. (2006b). Structure and receptor specificity of the hemagglutinin from an H5N1 influenza virus. Science *312*, 404–410.

Tong, Y.-G., Shi, W.-F., Liu, D., Qian, J., Liang, L., Bo, X.-C., Liu, J., Ren, H.-G., Fan, H., Ni, M., et al.; China Mobile Laboratory Testing Team in Sierra Leone (2015). Genetic diversity and evolutionary dynamics of Ebola virus in Sierra Leone. Nature *524*, 93–96.

Tscherne, D.M., Manicassamy, B., and García-Sastre, A. (2010). An enzymatic virus-like particle assay for sensitive detection of virus entry. J. Virol. Methods *163*, 336–343.

Urbanowicz, R.A., McClure, C.P., Sakuntabhai, A., Salle, A.A., Kobinger, G., Müller, M.A., Holmes, E.C., Rey, F.A., Simon-Loriere, E., and Ball, J.K. (2016). Human adaptation of Ebola virus during the West African outbreak. Cell *167*, this issue, 1079–1087.

Volchkov, V.E., Volchkova, V.A., Muhlberger, E., Kolesnikova, L.V., Weik, M., Dolnik, O., and Klenk, H.D. (2001). Recovery of infectious Ebola virus from complementary DNA: RNA editing of the GP gene and viral cytotoxicity. Science *291*, 1965–1969.

Wang, H., Shi, Y., Song, J., Qi, J., Lu, G., Yan, J., and Gao, G.F. (2016). Ebola viral glycoprotein bound to its endosomal receptor Niemann-Pick C1. Cell *164*, 258–268.

WHO (2016). Ebola Situation Reports | Ebola. http://apps.who.int/ebola/ebola-situation-reports (WHO).

Wickham, H. (2009). ggplot2: Elegant Graphics for Data Analysis (New York: Springer-Verlag).

Xu, R., McBride, R., Paulson, J.C., Basler, C.F., and Wilson, I.A. (2010). Structure, receptor binding, and antigenicity of influenza virus hemagglutinins from the 1957 H2N2 pandemic. J. Virol. *84*, 1715–1721.

Zhang, X.-Y., La Russa, V.F., Bao, L., Kolls, J., Schwarzenberger, P., and Reiser, J. (2002). Lentiviral vectors for sustained transgene expression in human bone marrow-derived stromal cells. Mol. Ther. *5*, 555–565.

Zhao, Y., Ren, J., Harlos, K., and Stuart, D.I. (2016). Structure of glycosylated NPC1 luminal domain C reveals insights into NPC2 and Ebola virus interactions. FEBS Lett. *590*, 605–612.

STAR★METHODS

KEY RESOURCES TABLE

REAGENT or RESOURCE	SOURCE	IDENTIFIER
Antibodies		
anti-CD14 antibody MicroBeads	Miltenyi	130-050-201
Rabbit anti-V5 polyclonal serum	Novus Biologicals	cat# NB600-381; RRID: AB_10001084
Mouse monoclonal anti-HIV p24 183-H12-5C	Chesebro et al., 1992; NIH AIDS Reagent Program	3537
goat anti-mouse-680	Li-Cor	925-68070
goat anti-rabbit-800	Li-Cor	925-32211
Chemicals, Peptides, and Recombinant Proteins		
Histopaque-1077	Sigma-Aldrich	H8889
RPMI-1640	ThermoFisher	11875119
DMEM, high glucose	ThermoFisher	11995073
EMEM	ATCC	30-2003
α-MEM	ThermoFisher	12571-063
Fetal Bovine Serum	Omega	FB-11
Human AB+ Serum	Omega Scientific	HS-20
HEPES	Corning	25-060-CI
MEM Non-Essential Amino Acids	Corning	25-025-CI
Sodium Pyruvate	Corning	25-000-CI
TransIT-LT1	Mirus Bio	MIR2306
cyclosporine A	Sigma	30024
Sucrose	Sigma	84097
TRIS-HCl	Corning	46-030-CM
NaCl	Sigma	S5150
EDTA	Corning	46-034-CI
NP40	Millipore	492016
Triton X-100	BioRad	161-0407
cOmplete mini protease inhibitor	Roche	11836170001
2-mercaptoethanol	Invitrogen	21985-023
Laemmli Buffer	BioRad	161-0737
4-20% gradient SDS-PAGE gels, 12 well	BioRad	456-1095
0.45 μM nitrocellulose membrane	BioRad	162-0112
TBS Odyssey Blocking Buffer	Li-Cor	927-50000
Critical Commercial Assays		
LiveBLAzer FRET-B/G Loading Kit with CCF4-AM	ThermoFisher	K1095
Deposited Data		
Public repository with clinical data	https://github.com/maxbiostat/diehl_ebola_cell_2016	N/A
Experimental Models: Cell Lines		
HEK293	ATCC	CRL-1573
U2OS	ATCC	HTB-96
S008842	Coriell Cell Repository	S008842
Vero	ATCC	CCL-81
FRhK4	ATCC	CRL-1688
CRFK	ATCC	CCL-94

(*Continued on next page*)

Continued		
REAGENT or RESOURCE	SOURCE	IDENTIFIER
Cf2Th	ATCC	CRL-1430
NIH/3T3	ATCC	CRL-1658
MDTF	Greg Towers	N/A
Recombinant DNA		
Plasmid backbone: pGL4.23-CMV	Modified from Promega	E8411
pAIP-hGMCSF-co	Reinhard et al., 2014; Addgene	74168
pAIP-hIL4-co	Reinhard et al., 2014; Addgene	74169
pNL-EGFP/CMV-WPREΔU3	Diehl et al., 2008; Addgene	17579
pCD/NL-BH*ΔΔΔ	Zhang et al., 2002; Addgene	17531
pcDNA3.1-Bla-VP40	BEI Resources	NR-19813
pLP/VSVG	ThermoFisher	N/A
pSIV3+	Nègre et al., 2000	N/A
Sequence-Based Reagents		
gBlock – EBOV GP ΔMLD	IDT; Chandran et al., 2005	N/A
Primer – GP_A82V-fwd: CAACTGACGTGCCATCTGTGACT AAAAGATGGGGCTTC	IDT; This paper	N/A
Primer – GP_A82V-rev: GAAGCCCCATCTTTTAGTCACAG ATGGCACGTCAGTTG	IDT; This paper	N/A
Primer – GP_T230A-fwd: CCGGTTTTGGAACTAATGAGG CAGAGTACTTGTTCGAGG	IDT; This paper	N/A
Primer – GP_T230A-rev: CCTCGAACAAGTACTCTGCCT CATTAGTTCCAAAACCGG	IDT; This paper	N/A
Primer – Primers: GP_D637G-fwd: GATAAAACCCTTCCG GGCCAGGGGGACAATGACAATTG	IDT; This paper	N/A
Primer – GP_D637G-rev: CAATTGTCATTGTCCCCCTGG CCCGGAAGGGTTTTATC	IDT; This paper	N/A
GBlock – V5 tag: […]TCTAGAGGTAAGCCTATCCCTAA CCCTCTCCTCGGTCTCGATTCTACGTAATCTAGA[…]	IDT; This paper	N/A
Primer – GP_delStop-fwd: CTGTATATGCAAATTTGTC TTTTCTAGAGTCGGGGCGGCC	IDT; This paper	N/A
Primer – GP_delStop-rev: GGCCGCCCCGACTCTAGA AAAGACAAATTTGCATATACAG	IDT; This paper	N/A
Software and Algorithms		
MAFFT	Katoh and Standley, 2013	v6.902b
trimA1	Capella-Gutiérrez et al., 2009	v1.4
RAxML	Stamatakis et al., 2005	v7.3.0
PRISM	GraphPad Software	Version 5
ICM-Pro	MolSoft	v3.8-5
R statistical package	R Core Team, 2016	v3.2.4
Databases		
Virus Pathogen Database and Analysis Resource (ViPR)	Pickett et al., 2012	Accessed July 2016

CONTACT FOR REAGENT AND RESOURCE SHARING

Further information and requests for reagents may be directed to the Lead Contact Jeremy Luban (jeremy.luban@umassmed.edu).

EXPERIMENTAL MODELS AND SUBJECT DETAILS

Cell Lines and Primary Human MDDCs

HEK293 (human [*Homo sapiens*] fetal kidney), U2OS (human [*Homo sapiens*] osteosarcoma), Vero (African green monkey [*Chlorocebus aethiops*] kidney), FRhk4 (rhesus macaque [*Macaca mulatta*] kidney), CRFK (cat [*Felis catus*] fetal kidney), Cf2Th (dog [*Canis*

familiaris] fetal thymus), and NIH/3T3 (house mouse [*Mus musculus*] embryonic fibroblast) cells were obtained from the ATCC (https://www.atcc.org/). S008842 (Chimpanzee [*Pan troglodytes*] skin fibroblast) cells were obtained from Coriell Cell Repository (Camden, NJ). MDTF (earth colored mouse [*Mus dunni*] tail fibroblast) cells were obtained from Greg Towers (UCL, London, UK). Cell lines were tested to verify the absence of mycoplasma. No assays were performed to verify the identity of the cells in culture following receipt of the cells. Peripheral blood mononuclear cells (PBMCs) were isolated from de-identified, healthy donor leukopaks (New York Biologics, Southampton, NY), in accordance with UMMS-IRB protocol ID #H00004971, which deems these cells non-human subjects research.

METHOD DETAILS

Sequence Data and Alignments

All publicly available EBOV Makona genomes were downloaded from the NIAID Virus Pathogen Database and Analysis Resource (ViPR) (Pickett et al., 2012) which can be accessed at https://www.viprbrc.org/ in July 2016 (n = 1,636; Table S1). Sequences with > 0.2% ambiguous or missing nucleotide calls were removed, and a high quality dataset of sequences was created comprising 1,489 coding-complete genomes (Table S2). Sequences were aligned with MAFFT v6.902b (Katoh and Standley, 2013) with the following parameters (L-INS-i):–localpair–maxiterate 1000–reorder–ep 0.123. Nucleotide alignments used for phylogenetic analyses were trimmed using trimAl v1.4 (Capella-Gutiérrez et al., 2009) with the maximum likelihood specific parameter: -automated1. Alignments of NPC1 amino acid sequences and EBOV Makona GP were also performed with MAFFT. Relevant alignments can be found in Data S1.

Phylogenetic Analysis

Maximum likelihood phylogenies were made with RAxML v7.3.0 (Stamatakis et al., 2005) using the GTRγ nucleotide substitution model. Fifty consecutive runs were performed and the tree with the best likelihood score was bootstrapped with 100 pseudoreplicates. To root the tree, all EBOV Makona sequences from Guinea were aligned with the 1976 EBOV Mayinga variant as an outgroup, which identified the earliest sequences from the 2013-2016 EVD epidemic as the most likely root of the tree (Data S1). All subsequent trees were rooted according to this analysis (Data S1).

Cell Culture

All cells were maintained at 37°C in 5% CO_2 humidified incubators. HEK293, U2OS, CRFK, NIH/3T3, and MDTF were maintained in DMEM supplemented with 10% FBS. S008842 were maintained in α-MEM supplemented with 15% FBS. Vero and FRhK4 were maintained in EMEM supplemented with 20% FBS. Cf2Th were maintained in DMEM supplemented with 20% FBS. HEPES pH 7.2-7.5 was added to all of these medium formulations at a final concentration of 10 mM. Mononuclear leukocytes were isolated by gradient centrifugation on Histopaque-1077 (Sigma-Aldrich, St. Louis, MO). $CD14^+$ mononuclear cells were enriched via positive selection using anti-CD14 antibody MicroBead conjugates (Miltenyi, San Diego, CA), according to the manufacturer's protocol. $CD14^+$ cells were then plated at a density of 1 to 2 × 10^6 cells/ml in RPMI-1640 supplemented with 5% heat inactivated human AB^+ serum (Omega Scientific, Tarzana, CA), 20 mM L-glutamine (ThermoFisher, Waltham, MA), 25 mM HEPES pH 7.2 (Sigma-Aldrich), 1 mM sodium pyruvate (ThermoFisher), and 1 x MEM non-essential amino acids (ThermoFisher). Differentiation of the $CD14^+$ monocytes into dendritic cells (MDDCs) was promoted by addition of recombinant human GM-CSF and human IL-4; cytokines were produced from HEK293 cells stably transduced with pAIP-hGMCSF-co or pAIP-hIL4-co, respectively, as previously described (Reinhard et al., 2014), with each cytokine supernatant added at a dilution of 1:100.

Plasmid DNA

Ebola virus glycoprotein from the Guinean reference strain (GenBank: KJ660346.2) was synthesized as a gBlock (Integrated DNA Technologies, Coralville, IA). It was engineered to lack the mucin domain (amino acids 309-489) (Chandran et al., 2005) and to contain an additional adenosine at nucleotide 890, a modification that substitutes for the transcriptional editing that bona fide EBOV uses to produce full-length glycoprotein (Sanchez et al., 1996). This sequence contained flanking NcoI and XbaI restriction enzyme sites and was cloned into a mammalian expression vector under the control of the cytomegalovirus immediate early (CMV IE) promoter/enhancer. Into this construct, A82V, T230A, and D637G single amino acid substitutions as well as A82V/T230A double and A82V/T230A/D637G triple amino acid substitutions were generated by QuikChange mutagenesis (Agilent Technologies, Santa Clara, CA), substituting in Phusion High-Fidelity PCR Master Mix with GC Buffer (New England Biolabs, Ipswich MA). The following primers were utilized for generating these mutations: A82V F: 5′-CAACTGACGTGCCATCTGTGACTAAAAGATGGGGCTTC-3′, A82V R: 5′-GAAGCCCCATCTTTTAGTCACAGATGGCACGTCAGTTG-3′, T230A F: 5′-CCGGTTTTGGAACTAATGAGGCAGAGTACTTGTTC GAGG-3′, T230A R: 5′-CCTCGAACAAGTACTCTGCCTCATTAGTTCCAAAACCGG-3′, D637G F: 5′-GATAAAACCCTTCCGGGC CAGGGGGACAATGACAATTG-3′, and D637G R: 5′-CAATTGTCATTGTCCCCCTGGCCCGGAAGGGTTTTATC-3′. Additional derivatives of the ancestral and mutant glycoproteins were generated by removal of the stop codon (F: 5′-CTGTATATGCAAAT TTGTCTTTTCTAGAGTCGGGGCGGCC-3′, R: 5′-GGCCGCCCCGACTCTAGAAAAGACAAATTTGCATATACAG-3′) and insertion of an XbaI-flanked C-terminal V5 tag synthesized as a gBlock (Integrated DNA Technologies).

Reporter Virus and Virus-like Particle Production

Viral stocks were generated by transfecting HEK293 cells using Mirus TransIT-LT1 lipid reagent, as follows (Mirus Bio, Madison, WI). 24 hr prior to transfection 6 × 10^5 HEK293 cells were plated per well in 6-well plates and transfected the following day with a total of 2,490 ng plasmid DNA using 6.25 μl TransIT-LT1 reagent. For production of pseudotyped EGFP-expressing HIV: 1,250 ng pNL-EGFP/CMV-WPREΔU3 (Diehl et al., 2008), 930 ng pCD/NL-BH*ΔΔΔ (Zhang et al., 2002), and 310 ng glycoprotein expression vector were utilized. For the production of pseudotyped ebola virus VLPs bearing beta-lactamase: 2,180 ng pcDNA3.1-Bla-VP40 (BEI Resources, Manassas, VA) (Manicassamy and Rong, 2009; Tscherne et al., 2010) and 310 ng glycoprotein expression vector were utilized. Whenever VSV-G pseudotypes were generated pLP/VSVG (ThermoFisher, Waltham, MA) was used to do so. Vpx-containing SIV VLPs were produced by transfecting 2180 ng pSIV3+ (Nègre et al., 2000) and 310 ng pLP/VSVG. Lentiviral VLPs for challenging DCs were produced by transfecting 2180 ng pCD/NL-BH*ΔΔΔ and 310 ng glycoprotein expression vector. In all cases, culture medium was changed 16 hr post transfection. In most cases fresh DMEM/10% FBS was used, but MDDC culture medium was utilized when virus was to be used for MDDC transductions. A further 48 hr after media change, viral supernatants were harvested, passed through a 0.45 μm pore size filter, and stored at 4°C.

Virus Infectivity Assays

For all adherent cells, 16 hr prior to transduction cells were seeded in 12 well plates at the following cell densities per well: HEK293 1x10^5; U2OS, FRhK4, CRFK, and NIH/3T3 3x10^4; S008842, Vero, Cf2Th, and MDTF 2x10^4. Cells were then exposed to virus-containing medium in a total volume of 350 μl for approximately 16 hr at 37°C. In order to relieve a TRIM5α block to infection (Berthoux et al., 2005), 8μg/ml cyclosporine A was added to the culture medium of FRhK4 and Vero cell lines. After this time, virus containing media was replaced with fresh culture medium and cells were cultured an additional 48 to 72 hr prior to harvest for flow cytometric analysis. For infection of THP-1 and human MDDCs, 5 × 10^5 cells were seeded per well of a 24-well plate at the time of infection and cells were exposed to virus-containing medium in a total volume of 200 μl for approximately 16 hr at 37°C. For MDDC infections, Vpx-containing VLPs were also added to the medium, in order to overcome a SAMHD1 block to viral infection (Laguette et al., 2011). After overnight culture in the presence of virus, fresh culture medium was added and cells were cultured an additional 48 to 72 hr prior to harvest for flow cytometric analysis.

Cells were harvested for flow cytometric analysis by trypsinization (all adherent lines) or scraping (MDDC), spun at 500 x *g* for 5 min, and resuspended in phosphate-buffered saline without Ca^{2+} and Mg^{2+}, supplemented with 2% FBS. Flow cytometry was conducted using the Accuri C6 system (BD Biosciences, San Jose, CA). Data was analyzed using FlowJo software, Macintosh version 10.1 (FlowJo, LLC, Ashland, OR). Infectivity of each mutant Ebola virus GP was compared to that observed with the ancestral GP, under the same conditions.

Infectivity Assay Using EBOV Virion Cores

Pseudotyped Ebola virus β-lactamase-VP40 (Bla-VP40) VLPs were prepared as described above. U2OS cells were seeded at a density of 1 × 10^5 cells per well in 96-well plates 16 hr prior to infection. For infections, growth medium was replaced with cold Bla-VP40 VLP-containing medium and incubated for 2 hr on ice. Virus containing medium was then removed and cells were washed once with ice cold Hank's Balanced Salt Solution (HBSS) and the cells were then incubated for 2 hr at 37°C in HBSS containing 10% FBS. Cells were then washed once with ice cold HBSS and loaded with the CCF4-AM substrate, according to the manufacturer's protocol (ThermoFisher) with the following modifications: the inhibitor of anion transport, probenecid, was added to a final concentration of 250 μM and cells were incubated with CCF4-AM substrate overnight at 11°C. Cleavage of the CCF4-AM substrate was assessed using the Synergy 2 plate reader (BioTek, Winooski, VT) with the following filter settings for the cleaved substrate: 400/30 excitation and 460/40 emission. The amount of CCF4-AM cleavage in cells infected with each mutant Ebola virus GP was compared to that observed for the ancestral GP, similar to what was done for infectivity assays.

Analysis of Clinical Data

In total there were 1,636 observations for which we had genotype information. Of these, only 194 cases were associated with both clinical outcome and C(t) value (viral load) information (Carroll et al., 2015; Gire et al., 2014; Quick et al., 2016). As the vast majority of these cases were from Guinea, we further restricted our attention to these 179 Guinean samples, as we did not want to introduce biases based on potential differences in the health care infrastructure or sample handling/processing. The 179 Guinean cases were used for all model fitting analyses. Maps depicting the spatial distribution of genotypes for all isolates and those associated with clinical outcome and viral load data were constructed using the maptools package (Bivand and Lewin-Koh, 2016). To obtain raw odds ratios, we tallied the number of individuals infected with genotype GP-A82V that died (a) and survived (b) and likewise for cases of individuals infected with genotype GP-A82 that died (c) and survived (d). The estimate for the raw odds ratio is then m = ad/bc. To compute confidence interval we calculated exp(m ± 1.96*S), where $S = \sqrt{1/a + (1/b) + (1/c) + (1/d)}$.

It is important, however, to control for the effect of other variables that might influence outcome in order to obtain adjusted odds ratios for the variable of interest (in this case, genotype). For each case we recorded the date of occurrence (in days since December 2013) and also the cumulative number of cases in the location of the case up to the date in which it was reported (cumCases). The idea behind acquiring this information was to detect any time-dependent trend in case fatality rates, as well as an overwhelming of the health care system due to a high case loads. We fit a binomial generalized linear model to the outcome data using these covariates

in addition to C(t) values and the absence/presence of the A82V mutation (genotype). In order to make coefficient estimates consistent between the continuous variables and the binary variable, we standardized the continuous variables by subtracting the mean and dividing by two standard deviations (Gelman, 2008). To facilitate interpretation of the results, we flipped the sign of the resulting variable such that it was consistent with viral load (which is inversely related to C(t)).

To further assess the effect of potential confounding variables, we fitted a varying-intercept (also called ''random effects'') model to the data where we assigned each location an intercept using the glmer() function in the lme4 package (Bates et al., 2015). This amounts to stating that each location was allowed to have its own baseline fatality rate. We also allowed each location to have its own coefficient for the cumCases variables, such that the structure of the model allowed for variability in how locations responded to demand for health care. Exploration of the model showed no association between sampling date and outcome and this variable was subsequently dropped of the model. The estimates for a model including C(t) values and genotype as ''fixed effects'' and cumCases are varying effect are presented in Figure S3 and show considerable uncertainty. We thus decided to make our inferences based on a simpler model, using only the fixed effect variables: C(t) and genotype.

A comparison of C(t) values per genotype was performed using a Student t test. Using all data for which C(t) values and genotype information was available (regardless of outcome information) we obtained 97 C(t) measurements for genotype GP-82A and 216 measurements for genotype GP-A82V. The results are reported in the main text and indicate no significant association between viral load (as measured by C(t)) and genotype.

All analyses were carried out in R 3.2.4 (R Core Team, 2016) and figures were produced using the ggplot2 package (Wickham, 2009).

Western Blots

For determination of Ebola virus GP incorporation into viral particles HEK293 cells were transfected according to the procedure above substituting plasmids encoding C-terminally V5-tagged Ebola virus GPs for the corresponding untagged versions. The V5-tagged constructs did indeed have the same phenotype as the untagged constructs (data not shown). 48 hr after media change, viral supernatant was harvested, passed through a 0.45μm filter, and layered over a 25% sucrose cushion. Virus was pelleted through the sucrose cushion by spinning at 125,000 x *g* using SW55Ti buckets in an Optima XE-90 ultracentrifuge (Beckman Coulter, Indianapolis, IN). Supernatant was removed and viral pellets were gently washed with 1 mL ice cold PBS. Virus was then lysed in Hypotonic Lysis Buffer: 20 mM TRIS-HCl, pH 7.5, 150 mM NaCl, 10 mM EDTA, 0.5% NP-40, 0.1% Triton X-100, and cOmplete mini protease inhibitor (Sigma-Aldrich, St. Louis, MO). Concomitantly, transfected cells were washed once with ice cold PBS and lysed in Hypotonic Lysis Buffer for 20 min on ice and clarified by centrifugation at 16,000 x g for 20 min at 4°C. Cell lysate supernatant was transferred to new tubes and insoluble pellets were discarded. In preparation for SDS-PAGE fractionation, viral and cellular lysates were mixed 1:1 with 2x Laemmli buffer containing 355 mM 2-mercaptoethanol and boiled for 5 min.

Prepared samples were run on 4%–20% gradient SDS-PAGE gels and transferred to nitrocellulose membranes. Membrane blocking, as well as both primary and secondary antibody binding were performed using TBS Odyssey Blocking Buffer (Li-Cor, Lincoln, NE), in accordance with the manufacturer's instructions. The V5 tag was detected using rabbit polyclonal serum (Novus Biologicals, Littleton, CO) at a 1:4,000 dilution. HIV-1 lentiviral CA (p24) was detected using mouse monoclonal antibody 183-H12-5C (Chesebro et al., 1992) at a 1:1,000 dilution. For imaging on the Li-Cor Odyssey CLx system (Li-Cor), primary antibody was recognized by goat anti-rabbit-680 and goat anti-mouse-800 (Li-Cor), both at 1:10,000 dilutions. Blots were scanned at a resolution of 84 μM using the 'medium quality' setting and quantitation of specific bands was done using the box tool in the Odyssey software package. Background subtraction was performed using pixels immediately adjacent to each box as reference background levels.

Protein Structure Modeling

Three-dimensional protein structure analysis, target-template alignments, and comparative homology modeling between human NPC1 bound to EBOV GPcl (experimentally derived by (Wang et al., 2016), Protein Data Bank accession number PDB: 5F1B) and targeted NPC1 loop 2 amino acid substitutions were performed using ICM-Pro version 3.8-5 (MolSoft, San Diego, CA; (Abagyan et al., 1994)).

QUANTIFICATION AND STATISTICAL ANALYSIS

Experimental n values, and information regarding what this refers to, can be found in the figure legends. Viral infectivity data for each cell line was independently assessed for statistical significance using Repeated-measures ANOVA, with values obtained from unique viral stocks being the variable considered for repeated-measures. For repeated-measures ANOVAs, a Dunnett's post-test for multiple comparisons was applied, where infectivity for all derivative GPs was compared to that of the ancestral GP. EBOV VLP fusion data was assessed for statistical significance using One-way Anova, with Bartlett's post-test comparing all derivative GPs to the ancestral GP. All ANOVAs were performed using PRISM 5 software (GraphPad Software, La Jolla, CA).

Cell

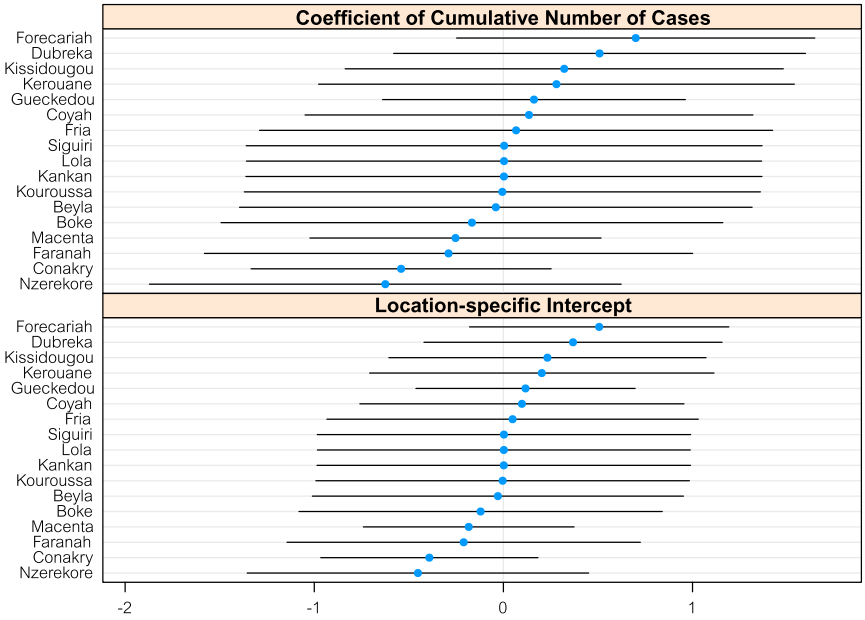

Figure S1. Varying-Intercept Model for Fatality Rates, Related to Figure 6

We fit a model that allowed each location to have its own base fatality rate (i.e., its own intercept) and also its own slope for the cumulative cases (cumCases) variable, in order to account for heterogeneity in how locations responded to demand for healthcare. We find that the variability in the data and possibly the relatively small number of observations lead to very broad estimates of the model parameters. While there seem to be differences in base fatality rate between Forecariah and Nzerekore for example, the overlap of confidence intervals precludes definitive conclusions.